Translational Motion Tracking of Leg Joints for Enhanced Prediction of Walking Tasks

Roman Stolyarov, Gary Burnett, and Hugh Herr, *Member, IEEE*

Abstract*—*Objective: **Walking task prediction in powered leg prostheses is an important problem in the development of biomimetic prosthesis controllers. This paper proposes a novel method to predict upcoming walking tasks by estimating the translational motion of leg joints using an integrated inertial measurement unit.** ***Methods:*** **We asked six subjects with unilateral transtibial amputations to traverse flat ground, ramps, and stairs using a powered prosthesis while inertial signals were collected. We then performed an offline analysis in which we simulated a real-time motion tracking algorithm on the inertial signals to estimate knee and ankle joint translations, and then used pattern recognition separately on the inertial and translational signal sets to predict the target walking tasks of individual strides.** ***Results:*** **Our analysis showed that using inertial signals to derive translational signals enabled a prediction error reduction of 6.8% compared to that attained using the original inertial signals. This result was similar to that seen by addition of surface electromyography sensors to integrated sensors in previous work, but was effected without adding any extra sensors. Finally, we reduced the size of the translational set to that of the inertial set and showed that the former still enabled a composite error reduction of 5.8%.** ***Conclusion and Significance:*** **These results indicate that translational motion tracking can be used to substantially enhance walking task prediction in leg prostheses without adding external sensing modalities. Our proposed algorithm can thus be used as a part of a task-adaptive and fully integrated prosthesis controller.**

***Index Terms*—Intent recognition, inertial measurement, machine learning, wearable robotics.**

I. Introduction

THE recent advent of powered leg prostheses has allowed modulation of control strategies depending on user actions. Such task-dependent actuation is important given the large variability in leg biomechanics between tasks such as level ground walking and ramp and stair traversal [1], [2]. While various advances have been made in prosthesis control methodologies within each of these tasks [3]–[6], a continuing area of research is to accurately and promptly predict transitions between tasks, and doing so without encumbering the user with devices external to their prosthesis.

The most effective walking task prediction methods to date have incorporated pattern recognition on signals obtained from a combination of integrated prosthesis sensors and external sensors such as wearable inertial measurement units (IMUs) [7], [8], optical distance sensors [9], [10], and surface electromyography (sEMG) electrodes [11]–[15]. While these attempts often resulted in accurate and prompt prediction of walking task across users, approaches based on external sensors encumber the user with additional sensor donning requirements and introduce performance dependency on donning technique and quality. Specifically for sEMG based approaches [11]–[13], [16]–[18], performance in a non-laboratory setting is uncertain because sEMG signals vary significantly with physiological factors including perspiration level [19], skin temperature [20], and subcutaneous fat thickness [21].

More integrated approaches have included combinations of inertial, mechanical, and kinetic sensors contained within the prosthetic assembly [22]–[25], but these methods *recognized* rather than *predicted* tasks, making most task determinations during or after ground contact. In a real-time controller, such delays would preclude anticipatory control decisions necessary to mimic biological gait such as plantarflexion for stair descent [26] or dorsiflexion for ground clearance in ascent tasks [26], [27].

Given the need for anticipating tasks and the disadvantages of relying on external sensors, an important goal is to predict tasks robustly using only integrated sensing modalities. In this work, we address this need by developing a novel and improved method for using an integrated IMU for walking task prediction. Previous work has shown that incorporating physiological sensors [11]–[14] or physiologically relevant signals [8], [15], [25] can enhance task prediction accuracy. In the same spirit, we aim to produce physiologically relevant signals, but relying instead on a non-physiological and mechanically integrated sensor. In our offline analysis, we employ signals from an IMU to generate physiologically meaningful estimates of leg joint translational motion and perform pattern recognition on the resulting signals to determine the target task of every stride. Our results demonstrate that this novel treatment of inertial

Manuscript received March 11, 2017; revised May 4, 2017; accepted June 9, 2017. Date of publication June 22, 2017; date of current version March 19, 2018. This work was supported by the United States Army Medical Research Acquisition Activity under Contract W81XWH-14-C-0111. The work of R. Stolyarov was supported in part by a National Defense Science and Engineering Graduate Fellowship and in part by the Harvard-MIT Health Sciences and Technology program. *(Corresponding author: Roman Stolyarov.)*

R. Stolyarov is with the Department of Health Sciences and Technology, Massachusetts Institute of Technology, Cambridge, MA 02139-4307 USA, and also with the Center for Extreme Bionics, Massachusetts Institute of Technology, Boston, MA 02139 USA (e-mail: romka@mit.edu).

G. Burnett is with the Department of Electrical Engineering and Computer Science, Massachusetts Institute of Technology.

H. Herr is with the Center for Extreme Bionics, Massachusetts Institute of Technology.

Digital Object Identifier 10.1109/TBME.2017.2718528

TABLE I
SUBJECT ATTRIBUTES

ID	Sex	Age	Ht(m)	Wt(kg)	Affected side
1	M	66	1.83	97	R
2	M	59	1.90	100	L
3	M	35	1.78	86	R
4	M	44	1.90	91	R
5	F	28	1.68	59	L
6	M	31	1.75	73	L

signals enables substantial performance improvement in walking task prediction, on par with that seen by the addition of external (sEMG) sensors to mechanical sensors in previous work [12]–[14], but effected without the addition of external sensors. The implication of our work is a method that can be combined with other integrated sensing modalities as part of a real-time task-adaptive leg prosthesis controller that is robust across users and physiological conditions.

II. METHODS

A. Data Collection

1) Overview: Six subjects with unilateral transtibial amputations (detailed subject attributes in Table I) and ability level K4 completed walking circuits along two terrain setups including a four-step staircase (0.17 m rise, 0.25 m run) and ramp (12-degree inclination, 2.0 m long) while wearing a powered ankle-foot prosthesis. Prosthesis sensor data and leg kinematics measured with motion capture were logged for offline processing. This study was approved by the Massachusetts Institute of Technology Institutional Review Board.

2) Equipment: Subjects completed all walking trials using the BiOM ankle-foot prosthesis (BionX Medical Technologies, Bedford, MA) coupled to a carbon composite foot of the subject's normally used size and stiffness. The assembly was attached to each subject's own custom fitted socket through a pylon of appropriate length. In each trial, sensor-frame acceleration ${}^S\vec{a}$ and rotational velocity ${}^S\vec{\omega}$ sampled from an integrated six-axis IMU (±6 g three-axis accelerometer, MMA7361LC; yaw rate gyroscope, ADXRS620; integrated dual-axis rate gyroscope, IDG500) and estimated ankle torque τ were remotely logged. All signals were sampled at 167 Hz.

A 12-camera Vicon 8i motion capture system with Vicon Nexus 1.8.5 was used to track subject kinematics relative to the terrains. This system was employed solely to facilitate automatic labeling of walking tasks for each trial.

3) Subject Preparation: Prior to completion of walking trials, the BiOM prosthesis assembly was aligned to each subject's custom fitted socket, and a foot cover and shoe were donned over the prosthetic foot. Prosthesis controller parameters were then tuned to the subject's particular gait biomechanics using a manufacturer provided wireless interface and tuning protocol. Subjects then practiced walking with the prosthesis for ten minutes.

Motion capture markers were applied to each subject's lower body segments and to all terrain setups sufficiently to enable automatic stride-by-stride labeling of walking task post data collection.

4) Walking Trials: Each subject completed multiple circuits at self-selected pace separately on a staircase setup and ramp setup. For both setups, each circuit comprised a flat ground traversal, terrain ascent, subsequent flat ground traversal on a level platform, and terrain descent. Stair traversal was performed in a step-over-step fashion. Prosthesis sensor signals were logged to a computer through a wireless transmitter and motion capture data was logged using the Vicon system. All trials were initiated with a three-second static standing period to allow calculation of a zero offset for gyroscope measurements and a gravity estimate from the accelerometers.

B. Offline Analysis

1) Overview: We compared the task prediction performance of sensed signals ${}^S\vec{a}$ and ${}^S\vec{\omega}$ to that of derived knee and ankle translational motion signals for a collection of strides extracted from the walking trials. Target walking tasks included flat ground walking (F), ramp ascent (RA), ramp descent (RD), stair ascent (SA), and stair descent (SD).

2) Trial Preprocessing: Marker trajectories were reconstructed from camera data using Vicon Nexus 1.8.5. Prosthesis sensor signals from each walking trial were low-pass filtered at 30 Hz. Marker trajectories were then manually synchronized to prosthesis sensor data by resampling the trajectories and manually aligning periods of elevated τ with periods of low horizontal velocity in prosthetic ankle markers.

3) Extraction of Individual Strides: Prosthesis and motion capture data from each trial was divided into individual strides i defined by an initial ground contact time $t_0^{(i)}$, foot-off time $t_{off}^{(i)}$, and subsequent ground contact time $t_0^{(i+1)}$. $t_0^{(i)}$, $t_{off}^{(i)}$, and $t_0^{(i+1)}$ were detected using a threshold on τ and each stride's target walking task was identified using motion capture data. Finally, strides from all trials were combined into one list, and those with short swing durations ($t_0^{(i+1)} - t_{off}^{(i)} \leq 400$ ms) were removed to filter small strides such as side-to-side shuffles or others that were not made in a predominantly forward direction. We selected a 400 ms cutoff to allow for retention of $>99\%$ of strides in the list while maximizing the size of the time window available for feature extraction.

4) Simulation of Motion Tracking Algorithm: We used a motion integration algorithm on ${}^S\vec{a}$ and ${}^S\vec{\omega}$ to estimate global-frame translational motion including ankle joint acceleration $\vec{a}_A$, knee joint acceleration $\vec{a}_K$ (combined here as $\vec{a}_{A,K}$), ankle and knee joint velocities $\vec{v}_{A,K}$, ankle and knee joint positions $\vec{p}_{A,K}$, and sensor-to-global frame rotation matrix R (Fig. 1). First, we calculated sensor-frame accelerations at the knee and ankle joints ${}^S\vec{a}_{A,K}$ from ${}^S\vec{a}$ and ${}^S\vec{\omega}$ using an equation for determining a point acceleration in a rigid body:

$$ {}^S\vec{a}_{A,K} = {}^S\vec{a} + {}^S\vec{\omega} \times {}^S\vec{\omega} \times {}^S\vec{r}_{A,K} + {}^S\dot{\vec{\omega}} \times {}^S\vec{r}_{A,K} \quad (1) $$

where ${}^S\vec{r}_{A,K}$ are the position vectors of the knee and ankle from the IMU in sensor frame and ${}^S\dot{\vec{\omega}}$ was low-pass filtered at 30 Hz.

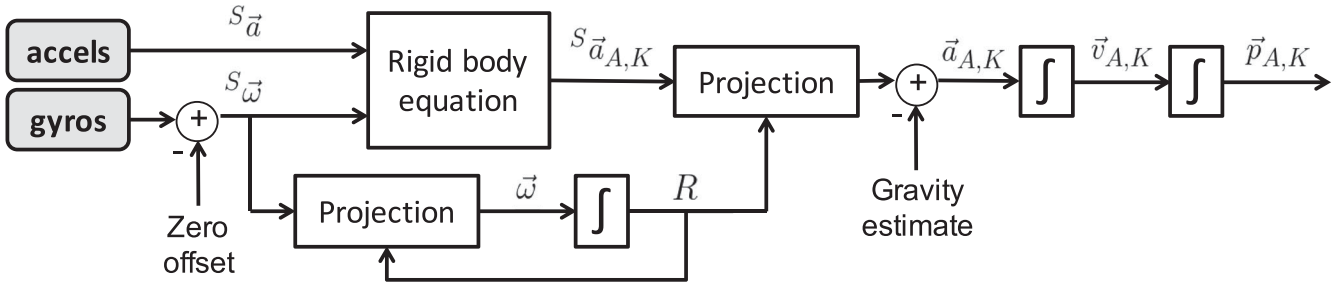

Fig. 1. Motion integration algorithm estimating knee and ankle translational motion $\vec{a}_{A,K}$, $\vec{v}_{A,K}$, and $\vec{p}_{A,K}$ and rotation matrix R using an IMU composed of accelerometers and gyroscopes. Zero offsets collected at the beginning of each trial are first subtracted from the gyroscope outputs producing $^S\vec{\omega}$, which is then projected onto global axes and integrated to calculate sensor-to-global frame rotation matrix R. $^S\vec{\omega}$ and $^S\vec{a}$ are used as input into the rigid body equation, which estimates sensor-frame accelerations at knee and ankle points $^S\vec{a}_{A,K}$. These are then projected onto global axes using R, adjusted by subtracting the gravity estimate to obtain $\vec{a}_{A,K}$, and integrated to obtain $\vec{v}_{A,K}$ and $\vec{p}_{A,K}$.

$^S\vec{r}_A$ was manufacturer provided, and $^S\vec{r}_K$ was calculated as:

$$^S\vec{r}_K = A^T[0;0;L] + {}^S\vec{r}_A \tag{2}$$

where A was a manufacturer provided sensor-to-prosthesis rotation matrix and L was shank length measured using motion capture. This calculation assumed that the prosthesis and residual shank frames were equivalent and that the knee joint was directly above the ankle joint in these frames. Next, we projected $^S\vec{a}_{A,K}$ onto global axes using R and subtracted the gravity estimate to attain global-frame joint accelerations $\vec{a}_{A,K}$. R was calculated by integrating $\vec{\omega}$, the global axis projection of $^S\vec{\omega}$. Finally, $\vec{a}_{A,K}$ was integrated twice to attain $\vec{v}_{A,K}$ and $\vec{p}_{A,K}$.

Due to bias in $^S\vec{a}$ and $^S\vec{\omega}$, integrated signals $\vec{v}_{A,K}$, $\vec{p}_{A,K}$, and R were subject to accumulating error. To bound this error, we reset these signals once near the beginning of each stride at an estimated foot-flat time $t_R^{(i)}$ at which the foot was presumed to be statically positioned against the terrain. Due to the absence of foot-ground strain sensors, we inferred $t_R^{(i)}$ as a time point when the prosthesis was close to vertical with the foot still on the ground:

$$t_R^{(i)} = \arg\max_t \left(\left| ||^P\vec{a}(t)|| - {}^P a_Z(t) \right| < \epsilon \right) \mid t \in [t_0^{(i)}, t_{off}^{(i)}] \tag{3}$$

where $^P\vec{a} = A^S\vec{a}$ and ϵ was a constant threshold. The $\arg\max$ function was used to find the latest possible $t_R^{(i)}$, thereby reducing the size of the interval $[t_R^{(i)}, t_{off}^{(i)}]$ for each stride and mitigating drift in velocity, position, and orientation estimates incurred prior to reaching swing phase. At $t_R^{(i)}$, integrated signals were reset by modeling the shank as a vertical lever rotating in the sagittal plane about a fixed hinge at the ankle joint:

$$\vec{p}_A(t_R^{(i)}) = \vec{v}_A(t_R^{(i)}) = [0;0;0] \tag{4}$$

$$\vec{p}_K(t_R^{(i)}) = [0;0;L] \tag{5}$$

$$\vec{v}_K(t_R^{(i)}) = [0; L\omega_X(t_R^{(i)}); 0] \tag{6}$$

$$R(t_R^{(i)}) = \mathbf{I} \tag{7}$$

where the components represent, in order, the frontal, anterior-posterior, and longitudinal axes.

5) Extraction of Feature Sets: For all strides, we created three separate feature sets including **S**(ensed), **T**(ranslational), and **E**(xpanded). All feature sets were comprised of the maxima, minima, means, and standard deviations extracted from associated signals in the window $[t_R^{(i)} : t_{off}^{(i)} + t_D]$ where $t_D = 400$ ms. **S** was extracted from $^S\vec{\omega}$ and $^S\vec{a}$ (6 signals total). **T** was extracted from sagittal plane translation signals including anterior-posterior and longitudinal components of $\vec{a}_{A,K}$, $\vec{v}_{A,K}$, and $\vec{p}_{A,K}$, as well as shank pitch angle and velocity, computed using Euler angle conversion on the prosthesis-to-global rotation matrix $P = RA^T$ (14 signals total). Non-sagittal translation signals were excluded from **T** to reduce feature set size and were based on the assumption that walking mechanics occur predominantly in the sagittal plane. Finally, **E** contained both features of **S** and features extracted from integrated and differentiated $^S\vec{\omega}$ and $^S\vec{a}$ (18 signals total, differentiated signals were low-pass filtered at 30 Hz). **E** was included as a control because we expected that naively increasing the number of generated signals would improve pattern recognition accuracy, yet we were specifically interested in determining the utility of translations. All feature sets were normalized to zero mean and unit variance across all strides.

6) Task Prediction Analysis With Fixed Cutoff: For **S**, **E**, and **T**, we performed cross validation using linear discriminant analysis (LDA) on 20 randomly generated, approximately equally sized folds (19 folds in the training set, 1 fold in the test set, repeated such that each fold was the test set once). All LDA training was performed using uniform priors and cost matrix.

Error metrics were calculated based on the combined prediction vector from all 20 folds given knowledge of the actual target tasks of each stride. In particular, we report three error metrics: "composite" (calculated on all strides), "transitional" (calculated on strides with different initial and final tasks), and "steady state" (calculated on strides with the same initial and final tasks). We performed one-way ANOVAs for all error metrics, followed by a post-hoc Tukey test to verify performance differences between feature sets. We also report numerical confusion matrices for each feature set.

7) Task Prediction Analysis With Variable Cutoff: Next, we repeated the cross validation analysis for **S**, **E**, and **T** generated with different cutoff times t_D to determine the

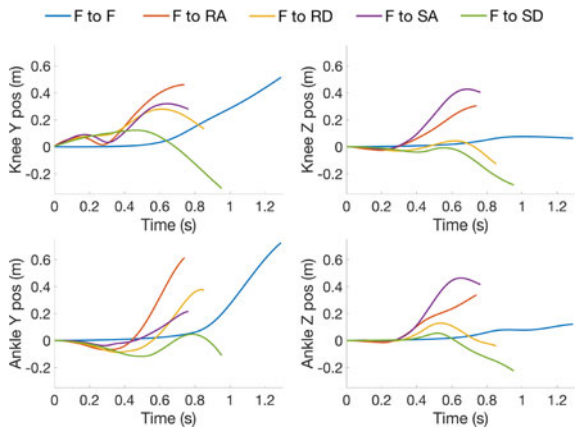

Fig. 2. Knee and ankle anterior-posterior (*Y*) and longitudinal (*Z*) position signals calculated using an IMU for five representative strides made by the same subject with different task transitions. All plotted strides except flat-to-flat were led by the biological leg. Signals are plotted for the window $[t_R^{(i)} : t_0^{(i+1)}]$ to show behavior for the entire stride. Knee *Z* position is displayed offset by the subject's shank length to allow easy comparison between axes.

consistency of the observed performance differences between feature sets. We report composite errors attained by $\mathbf{S}$, $\mathbf{E}$, and $\mathbf{T}$ extracted from signals in the window $[t_R^{(i)} : t_{off}^{(i)} + t_D]$ for values of t_D from 0 ms to 400 ms in increments of 50 ms.

8) Feature Reduction: We were interested in ranking the predictive power of signals of $\boldsymbol{T}$ in order of marginal composite error reduction and determining whether we could reduce the size of $\boldsymbol{T}$ to that of $\boldsymbol{S}$ and still observe a significant improvement in prediction accuracy. Thus, we performed forward selection of signals in $\boldsymbol{T}$ by minimizing composite error from 20-fold cross validation for $t_D = 400$ ms.

III. Results

A. Generated Stride List

The generated stride list included a total of 1541 strides, with 66% of strides ending in F, 7% in RA, 7% in RD, 10% in SA, and 10% in SD.

B. Translational Signals

Representative examples of calculated knee and ankle sagittal translations from strides included in the analysis are shown in Fig. 2. Deviations from expected anterior-posterior trajectories for the represented terrains are caused by integration error in orientation estimation, which can cause horizontal acceleration artifact due to gravity. Additionally, net loss in horizontal knee position during stair descent can be explained by the tendency of some subjects to descend stairs sideways, likely to face the railing.

C. Task Prediction Analysis With Fixed Cutoff

Prediction error metrics for $\boldsymbol{S}$, $\boldsymbol{E}$, and $\boldsymbol{T}$ are displayed in Fig. 3. All error metrics were significantly lower for E compared to S, and for T compared to S or E ($p < 0.05$). In particular, training with T instead of S enabled composite, transitional, and steady state error reductions of 6.8%, 12.4%, and 4.9%, respectively, while training with E instead of S enabled corresponding reductions of 4.3%, 6.7%, and 3.5%. As a metric of performance consistency across subjects, we determined the maximum composite error for an individual subject for the three feature sets. Respectively for S, E, and T, these errors were 19.1%, 9.3%, and 5.9%.

We also report confusion matrices for each feature set, (Table II). These matrices show that the composite error differences between feature sets can primarily be accounted for by differences in ramp prediction error. Compared to S, ramp ascent and descent prediction accuracies respectively improved by 17.2% and 24.2% when using E and by 30.8% and 40.9% when using T. Despite these differences, ramp tasks were the least accurately predicted tasks for all feature sets. Accuracy was consistently high ($\geq$94%) for flat ground and stair task prediction, although higher for E and T than for S.

D. Task Prediction Analysis With Variable Cutoff

We report the composite error performance of all feature sets in Fig. 4. Independently of cutoff t_D, classifiers trained using T performed significantly better than those trained using S ($p < 0.01$ for all t_D). Compared to E, T achieved significant error reduction for $t_D \geq 250$ ms ($p < 0.01$).

E. Feature Reduction

The full results of forward signal selection are shown in Fig. 5. We observed $\geq 1\%$ marginal composite error reduction with the selection of the first 5 signals (knee vertical position, pitch velocity, ankle vertical acceleration, ankle horizontal velocity, and pitch angle) from T and reductions of $\leq 0.25\%$ per signal thereafter. The error attained using the first 6 signals, equal to the amount used to create S, was significantly lower than the composite error of S ($p \leq 0.01$). Furthermore, only the first 2 selected signals from T were needed to enable a significant error reduction from S ($p \leq 0.05$). Finally, 7 out of the 15 signals used to make T were needed to attain a composite error that was not significantly different from that of T.

IV. Discussion

A. Summary

In this study, we analyzed the performance of stride-by-stride walking task prediction in a transtibial prosthesis using different treatments of signals from an IMU. Our results demonstrate that prediction using inertial signals can be performed more accurately and with fewer features when these signals are first transformed into estimates of leg joint translations. This improvement is greater than that enabled by a naive expansion of the inertial signal set, indicating the particularly informative value of translation signals.

B. Advantages of the Proposed Method

Several qualities of the proposed method might underlie its effectiveness in predicting user behavior. The first is that

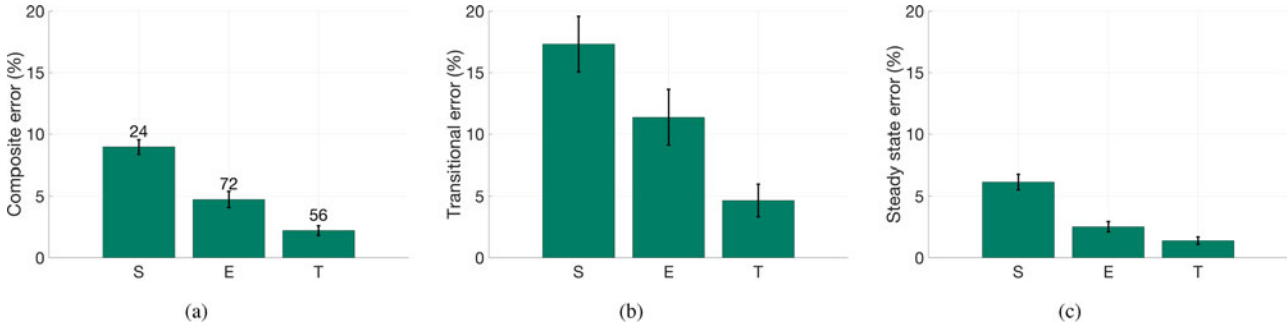

Fig. 3. Error metrics from 20-fold cross-validation of LDA classifiers built on feature sets S(ensed), E(xpanded), and T(ranslational) extracted from signals in the window $[t_R^{(i)} : t_{off}^{(i)} + t_D]$ for $t_D = 400$ ms. Error bars represent ± 1 SEM. (a) Composite error of the prediction vector combined from all folds. Numbers above error bars represent the total feature count of each set. (b) Transitional error of the prediction vector combined from all folds. (c) Steady state error of the prediction vector combined from all folds.

TABLE II
CONFUSION MATRICES OF 20-FOLD LDA CROSS VALIDATION

		Predicted mode–(S)ensed					Predicted mode–(E)xpanded					Predicted mode–(T)ranslational				
		F	RA	RD	SA	SD	F	RA	RD	SA	SD	F	RA	RD	SA	SD
Target mode	**F**	96.0	1.6	1.8	0.2	0.5	97.8	0.8	1.1	0.0	0.4	98.7	0.4	0.8	0.0	0.1
	RA	37.0	59.3	0.0	3.7	0.0	23.5	76.5	0.0	0.0	0.0	9.9	90.1	0.0	0.0	0.0
	RD	42.5	0.0	53.3	0.0	4.2	20.8	0.0	77.5	0.0	1.7	5.8	0.0	94.2	0.0	0.0
	SA	0.0	1.9	0.0	98.1	0.0	0.0	0.6	0.0	99.4	0.0	0.0	0.0	0.0	100.0	0.0
	SD	0.0	0.0	5.1	0.0	94.9	0.0	0.0	1.3	0.0	98.7	0.6	0.0	1.3	0.0	98.1

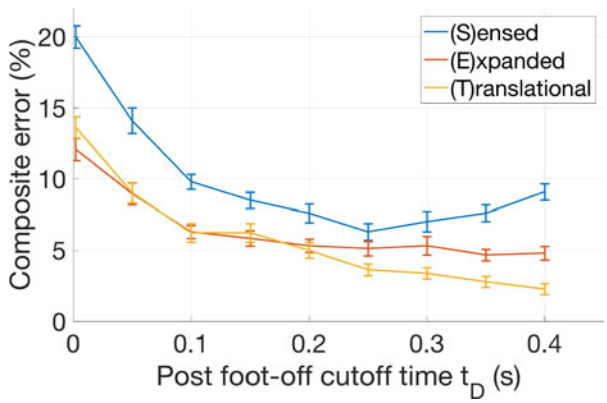

Fig. 4. Effect of signal cutoff time post foot-off on the composite error from 20-fold cross validation attained by the S(ensed), E(xpanded), and T(ranslational) feature sets. Error bars represent ± 1 SEM.

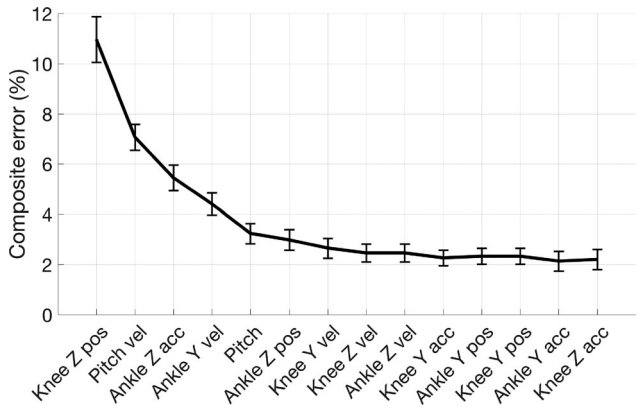

Fig. 5. Effect of sequential addition of signals used to make the T(ranslational) feature set on composite error. Signals were selected based on a sequential forward search where performance for each signal set was measured by the composite error from 20-fold cross validation. The resulting selection is displayed from left to right on the graph. *Y* signals are anterior-posterior components and *Z* signals are longitudinal components. Error bars represent ± 1 SEM.

translational signals directly describe volitionally controlled user actions, and in particular knee and ankle joint movement through muscular activation. By incorporating knowledge of leg skeletal structure and human walking in addition to the sensed inertial signals, translational signals provide information not only about prosthetic state but also about physiological state. This idea builds on results of former studies on walking task prediction, which have concluded that the addition of sEMG signals to intrinsic prosthesis measurements significantly improves task prediction accuracies.

In addition to their connection with human behavior, joint translation signals also directly reflect terrain geometry. Given accurate estimates of joint translations, this geometrical coupling guarantees that certain signal qualities will be observed given terrain transitions independently of walking speed, prosthesis, or the controller state. For example, knee altitude during step-over-step stair traversal necessarily changes by at least two stair heights every stride. Indeed, as shown in Fig. 5, knee altitude was identified as the single most informative signal in the translational set by the signal selection process, likely due to its close geometrical coupling with terrain variation.

Correspondence between translation signals and target terrain geometry is further supported by Fig. 4, which indicates that translational signals are especially advantageous for later cutoff times (in particular, 250 ms to 400 ms). Because the target terrain defines a particular region suitable for ground contact, it makes sense that the target terrain identity becomes more evident as the leg joints tend toward and eventually reach this region.

Joint translation signals are also more intuitive than inertial signals, meaning that the resulting task predictor has easily interpretable features. This introduces the potential for a modular prediction algorithm that can be tuned for specific differences across users or specific terrain geometries without further data collection and classifier training. The performance improvement attained using just a small number of translation signals also speaks to the possibility of a prediction model that is generalized, intuitive, and tunable.

The proposed method is also computationally feasible for real-time implementation, as evidenced by the widespread use of IMUs in real-time motion tracking applications. For illustration, the algorithm in Fig. 1 requires ~ 100 floating point operations (FLOPs) per sample. Given a sampling rate of ~ 100 Hz required to capture most signal power in walking [28], this motion tracking algorithm would require $\sim 10,000$ FLOPs per second, well within modern microprocessing capability. Final task classification, performed once per stride, would require small computational overhead given a small feature count.

Finally, this method would likely also be useful for enhancing prediction accuracy in transfemoral prostheses, where it is possible to inertially track not only knee and ankle but also hip motion using knowledge of foot-flat and joint angles. We conducted a preliminary analysis by using only signals of knee translational motion (volitionally controlled by transfemoral amputees during swing) to predict walking mode and attained a composite error of 4.7%. It is likely this value would improve with knowledge of hip translations, but this would have to be investigated empirically.

C. Potential Improvements and Limitations

The primary novelty of this study is the specific method of treating inertial signals in a prosthesis to improve determination of the user's current and future actions. However, it is likely that the addition of other sensing modalities would further enhance the ability to infer user intent, and that the accuracies presented in this work are not the highest attainable employing the proposed method. Therefore, the primary potential improvement of this method is combination with other integrated sensors, including kinetic, kinematic, or additional inertial devices.

It is also likely that reduction or elimination of common error sources of motion tracking with inertial sensors would further improve prediction accuracy. The two primary sources of error for these measurements as performed in this study were incorrect initial estimation of shank orientation and accumulating integration error. The first effect can be minimized by directly detecting rather than inferring the foot-flat phase using foot-ground strain sensing. The second effect can be minimized by using drift compensation algorithms such as Kalman or particle filters.

Finally, potential limitations of the method include diminished performance at slow walking speeds, which would allow greater drift in translation estimates, and in any situations that might not permit a completely static ankle at foot-flat, such as soft, slippery, or otherwise dynamic surfaces.

V. Conclusion

We have demonstrated a novel algorithm to use integrated mechanical sensors for walking task prediction in lower limb prostheses. In an offline analysis, we used pattern recognition to show that task prediction using inertial measurement could be performed more accurately and with fewer predictor features if the inertial measurements were first used to track the translational motion of the user's ankle and knee joints. These results indicate that walking task prediction can be enhanced not only by physiological sensors as shown in previous work, but also by physiologically informative signals. Our method's high accuracy across users and small feature count suggest that it would generalize to settings outside of the laboratory.

Acknowledgment

The authors would like to acknowledge R. Emerson for prosthetic fitting, M. Eilenberg for technical support, M. Orton for help with data collection, T. Clites for consultation on study planning and execution, and all subjects who participated in the study.

References

[1] S. D. Prentice *et al.*, "Locomotor adaptations for changes in the slope of the walking surface," *Gait Posture*, vol. 20, no. 3, pp. 255–265, Dec. 2004.
[2] B. J. McFadyen and D. A. Winter, "An integrated biomechanical analysis of normal stair ascent and descent," *J. Biomech.*, vol. 21, no. 9, pp. 733–744, Jan. 1988.
[3] J. Markowitz *et al.*, "Speed adaptation in a powered transtibial prosthesis controlled with a neuromuscular model," *Phil. Trans. Roy. Soc. B: Biol. Sci.*, vol. 366, no. 1570, pp. 1621–1631, Apr. 2011.
[4] H. M. Herr and A. M. Grabowski, "Bionic ankle-foot prosthesis normalizes walking gait for persons with leg amputation," *Proc. Roy. Soc. B: Biol. Sci.*, vol. 279, no. 1728, pp. 457–464, Jul. 2011.
[5] B. Lawson *et al.*, "Control of stair ascent and descent with a powered Transfemoral Prosthesis," *IEEE Trans. Neural Syst. Rehabil. Eng.*, vol. 21, no. 3, pp. 466–473, May 2013.
[6] N. P. Fey *et al.*, "Controlling knee swing initiation and ankle Plantarflexion with an active prosthesis on level and inclined surfaces at variable walking speeds," *IEEE J. Transl. Eng. Health Med.*, vol. 2, pp. 1–12, 2014.
[7] M. Gorsic *et al.*, "Online phase detection using Wearable sensors for walking with a robotic prosthesis," *Sensors*, vol. 14, no. 2, pp. 2776–2794, Feb. 2014.
[8] L. Ambrozic *et al.*, "CYBERLEGs: A user-oriented robotic Transfemoral Prosthesis with whole-body awareness control," *IEEE Robot. Autom. Mag.*, vol. 21, no. 4, pp. 82–93, Dec. 2014.
[9] M. Liu *et al.*, "Development of an environment-aware Locomotion mode recognition system for powered lower limb Prostheses," *IEEE Trans. Neural Syst. Rehabil. Eng.*, vol. 24, no. 4, pp. 434–443, Apr. 2016.
[10] F. Zhang *et al.*, "Preliminary design of a terrain recognition system," in *Proc. Annu. Int. Conf. IEEE Eng. Med. Biol. Soc.*, 2011, pp. 5452–5455.
[11] H. Huang *et al.*, "Continuous locomotion-mode identification for Prosthetic legs based on neuromuscular-mechanical fusion," *IEEE Trans. Biomed. Eng.*, vol. 58, no. 10, pp. 2867–2875, Oct. 2011.
[12] L. J. Hargrove and D. C. Tkach, "Neuromechanical sensor fusion yields highest accuracies in predicting ambulation mode transitions for transtibial amputees," in *Proc. Annu. Int. Conf. IEEE*, 2013, pp. 3074–3077.

[13] A. J. Young *et al.*, "Analysis of using EMG and mechanical sensors to enhance intent recognition in powered lower limb prostheses," *J. Neural Eng.*, vol. 11, no. 5, Sep. 2014, Art. no. 056021.
[14] L. J. Hargrove *et al.*, "Intuitive control of a powered prosthetic leg during ambulation," *JAMA*, vol. 313, no. 22, pp. 22–44, 2015.
[15] J.A. Spanias *et al.*, "Effect of additional mechanical sensor data on an EMG-based pattern recognition system for a powered leg prosthesis," in *Proc. Int. IEEE/EMBS Conf. Neural Eng.*, 2015, pp. 639–642.
[16] H. Huang *et al.*, "A strategy for identifying locomotion modes using surface Electromyography," *IEEE Trans. Biomed. Eng.*, vol. 56, no. 1, pp. 65–73, Jan. 2009.
[17] D. Jin *et al.*, "Terrain identification for prosthetic knees based on electromyographic signal features," *Tsinghua Sci. Technol.*, vol. 11, no. 1, pp. 74–79, Feb. 2006.
[18] E. Ceseracciu *et al.*, "SVM classification of locomotion modes using surface electromyography for applications in rehabilitation robotics," in *Proc. IEEE Int. Symp. Robot Hum. Interact. Commun.*, 2010, pp. 165–170.
[19] M. Abdoli-Eramaki *et al.*, "The effect of perspiration on the sEMG amplitude and power spectrum," *J. Electromyography Kinesiology*, vol. 22, no. 6, pp. 908–913, Dec. 2012.
[20] J. Winkel and K. Jorgensen, "Significance of skin temperature changes in surface electromyography," *Eur. J. Appl. Physiol. Occup. Physiol.*, vol. 63, no. 5, pp. 345–348, Nov. 1991.
[21] C. Nordander *et al.*, "Influence of the subcutaneous fat layer, as measured by ultrasound, skinfold calipers and BMI, on the EMG amplitude," *Eur. J. Appl. Physiol.*, vol. 89, no. 6, pp. 514–519, Aug. 2003.
[22] Y. D. Li and E. T. Hsiao-Wecksler, "Gait mode recognition and control for a portable-powered ankle-foot orthosis," in *Proc. IEEE Int. Conf. Rehabil. Robot.*, 2013.
[23] X. Wang *et al.*, "A wearable plantar pressure measurement system: Design specifications and first experiments with an amputee," in *Proc. Int. Conf. Intell. Auton. Syst.*, 2012, pp. 273–281.
[24] B. Chen *et al.*, "A foot-wearable interface for locomotion mode recognition based on discrete contact force distribution," *Mechatronics*, vol. 32, 2015.
[25] K. Yuan *et al.*, "Fuzzy-logic-based terrain identification with multisensor fusion for transtibial Amputees," *IEEE/ASME Trans. Mechatronics*, vol. 20, no. 2, pp. 618–630, Apr. 2015.
[26] Sinitski "Biomechanics of the ankle-foot system during stair ambulation: Implications for design of advanced ankle-foot prostheses," *J. Biomech.*, vol. 45, no. 3, pp. 588–594, 2012.
[27] A. S. McIntosh *et al.*, "Gait dynamics on an inclined walkway," *J. Biomech.*, vol. 39, no. 13, pp. 2491–2502, 2006.
[28] E. Munoz Diaz *et al.*, "Optimal sampling frequency and bias error modeling for foot-mounted IMUs," in *Proc. IEEE Int. Conf. Indoor Positioning Indoor Navig.*, 2013, pp. 1–9.